








# Excessive nucleic acid R-loops induce mitochondria-dependent epithelial cell necroptosis and drive spontaneous intestinal inflammation

Xu Yang<sup>a,b,c,1</sup>, Guilin Li<sup>a,b,1</sup>, Pengbo Lou<sup>d</sup>, Mingxin Zhang<sup>b</sup>, Kai Yao<sup>b</sup>, Jintao Xiao<sup>e,f</sup>, Yiqian Chen<sup>e,f</sup> , Jiuzhi Xu<sup>b</sup>, Shengyuan Tian<sup>b</sup>, Min Deng<sup>b</sup>, Yuwei Pan<sup>b</sup>, Mengzhen Li<sup>b</sup>, Xi Wu<sup>b</sup>, Ruiqi Liu<sup>b</sup>, Xiaojing Shi<sup>a</sup>, Yuhua Tian<sup>a</sup>, Lu Yu<sup>b</sup>, Hao Ke<sup>b</sup>, Baowei Jiao<sup>b</sup> , Yingzi Cong<sup>h</sup> , Maksim V. Plikus<sup>i</sup> , Xiaowei Liu<sup>e,f,2</sup>, Zhengquan Yu<sup>a,b,2</sup> , and Cong Lv<sup>j,2</sup>

Edited by Robb Krumlauf, Stowers Institute for Medical Research, Kansas City, MO; received May 4, 2023; accepted November 21, 2023

Oxidative stress, which can be activated by a variety of environmental risk factors, has been implicated as an important pathogenic factor for inflammatory bowel disease (IBD). However, how oxidative stress drives IBD onset remains elusive. Here, we found that oxidative stress was strongly activated in inflamed tissues from both ulcerative colitis patients and Crohn's disease patients, and it caused nuclear-to-cytosolic TDP-43 transport and a reduction in the TDP-43 protein level. To investigate the function of TDP-43 in IBD, we inducibly deleted exons 2 to 3 of *Tardbp* (encoding Tdp-43) in mouse intestinal epithelium, which disrupted its nuclear localization and RNA-processing function. The deletion gave rise to spontaneous intestinal inflammation by inducing epithelial cell necroptosis. Suppression of the necroptotic pathway with deletion of *Mkl1* or the *RIP1* inhibitor *Nec-1* rescued colitis phenotypes. Mechanistically, disruption of nuclear TDP-43 caused excessive R-loop accumulation, which triggered DNA damage and genome instability and thereby induced *PARP1* hyperactivation, leading to subsequent  $\text{NAD}^+$  depletion and ATP loss, consequently activating mitochondrion-dependent necroptosis in intestinal epithelial cells. Importantly, restoration of cellular  $\text{NAD}^+$  levels with  $\text{NAD}^+$  or *NMN* supplementation, as well as suppression of *ALKBH7*, an  $\alpha$ -ketoglutarate dioxygenase in mitochondria, rescued TDP-43 deficiency-induced cell death and intestinal inflammation. Furthermore, TDP-43 protein levels were significantly inversely correlated with  $\gamma$ -H2A.X and p-MLKL levels in clinical IBD samples, suggesting the clinical relevance of TDP-43 deficiency-induced mitochondrion-dependent necroptosis. Taken together, these findings identify a unique pathogenic mechanism that links oxidative stress to intestinal inflammation and provide a potent and valid strategy for IBD intervention.

inflammatory bowel disease | necroptosis | TDP-43 | R-loop

Inflammatory bowel disease (IBD), a chronic inflammatory disorder in the intestines, includes ulcerative colitis (UC) and Crohn's disease (CD) (1). Oxidative stress is a common feature of inflamed tissues from IBD patients. Oxidative stress can be activated by a variety of environmental risk factors, such as psychological stress, cigarette smoking, and alcohol, all of which contribute to IBD. Mutations in antioxidant/biotransformation enzyme genes, including *NOQ1*, *SOD2*, *GST*, *PON*, and *NRF2*, are associated with IBD progression (2–4). Oxidative stress and redox signaling up-regulate inflammatory cytokines by regulating the proinflammatory NF- $\kappa$ B signaling pathway (5). Oxidative stress also contributes to IBD pathogenesis by regulating lipid peroxidation and oxidative DNA damage (6). Despite significant efforts to understand the role of oxidative stress in IBD pathogenesis, whether it is a critical driver of the onset of intestinal inflammation remains elusive.

Necroptosis is a caspase-independent form of programmed cell death that can be activated by excessive DNA damage or exposure to virus-derived Z-DNA (7). It is mainly considered as a type of proinflammatory cell death due to the release of damage-associated molecular patterns (8), which can activate immune response and promote inflammation. Increasing evidence indicates that necroptosis plays important role in the pathogenesis of IBD. Aberrant necrotic cell death activation and upregulation of the key necroptosis effector *RIPK3* have been observed in both pediatric and adult IBD (9, 10). Necroptosis in intestinal epithelial cells induces spontaneous ileitis and/or colitis (9, 11). Furthermore, hyperactivation of mammalian target of rapamycin or *Setd1* loss-induced genome instability can trigger necroptotic activation that drives intestinal inflammation and cancer (12, 13). Targeting necroptotic pathway might represent a promising therapeutic strategy for IBD. Various inhibitors of necroptosis have been suggested to alleviate intestinal inflammation (14–16). Although the importance of necroptosis in IBD has been realized,

## Significance

Inflammatory bowel disease (IBD) is a chronic inflammatory disorder in the intestines. As the etiology of IBD remains largely unknown, this disease lacks effective therapeutic approach. Oxidative stress is a feature of IBD, yet surprisingly little is known about the molecular mechanism that links oxidative stress to this disease. In this work, we found that oxidative stress induces nucleus-to-cytosol transport of TDP-43, and its mislocalization causes excessive nucleic acid R-loops that induce spontaneous intestinal inflammation by activating  $\text{NAD}^+$  depletion-induced mitochondrion-dependent necroptosis. Consequently, supplementation with  $\text{NAD}^+$  and its precursor *NMN* significantly alleviates the colitis phenotypes. This work identifies a new mechanism that underpins oxidative stress-driven intestinal inflammation and provides proof of principle that *NMN* is a viable therapeutic approach for IBD.

The authors declare no competing interest.

This article is a PNAS Direct Submission.

Copyright © 2023 the Author(s). Published by PNAS. This article is distributed under [Creative Commons Attribution-NonCommercial-NoDerivatives License 4.0 \(CC BY-NC-ND\)](https://creativecommons.org/licenses/by-nc-nd/4.0/).

<sup>1</sup>X.Y. and G.L. contributed equally to this work.

<sup>2</sup>To whom correspondence may be addressed. Email: liuxw@csu.edu.cn, zyu@zsu.edu.cn, zyu@cau.edu.cn, or lvc@cau.edu.cn.

This article contains supporting information online at <https://www.pnas.org/lookup/suppl/doi:10.1073/pnas.2307395120/-/DCSupplemental>.

Published December 29, 2023.

it remains unknown whether and how necroptosis is activated upon environmental risk factor-induced oxidative stress and thereby induces intestinal inflammation.

The R-loop is a three-stranded nucleic acid structure consisting of the RNA:DNA hybrid that occurs in association with transcription and replication. It has been linked to several human diseases, including autoimmune diseases and human neurological disorders (17). Excessive R-loops give rise to DNA damage and genome instability, which contribute to the development of the above diseases (18). Interestingly, TDP-43 dysfunction results in R-loop accumulation and links amyotrophic lateral sclerosis (ALS) with R-loop-mediated DNA damage (19–21). However, the pathogenic functions of TDP-43-mediated R-loop accumulation in IBD have not been investigated. Here, we demonstrate that nucleus-to-cytosol TDP-43 mislocalization causes excessive R-loops to activate epithelial cell necroptosis, mediating oxidative stress-driven intestinal inflammation.

## Results

**TDP-43 Exhibits Nucleus-to-Cytosol Mislocalization in Inflamed IBD Epithelial Cells upon Oxidative Stress.** To study potential causative roles of oxidative stress in driving IBD pathogenesis, we first examined oxidative status of inflamed tissues from IBD patients. Immunohistochemical staining for COX2 and NOX2, biochemical markers for oxidative stress, showed both markers broadly upregulated in inflamed epithelium from both UC and CD patients (Fig. 1*A* and *SI Appendix, Fig. S1 A–C*). G3BP1 is a stress granule marker, and its immunostaining showed extensive formation of stress granules in the inflamed epithelium from both UC and CD patients, while stress granules were prominently absent in normal intestinal epithelium (Fig. 1*B* and *SI Appendix, Fig. S1D*).

It has been reported that TDP-43 becomes transported from nucleus to cytosol upon oxidative stress and participates in stress granule formation (22). Indeed, TDP-43 colocalized with G3BP1 to form stress granules in inflamed epithelium from IBD patients and exhibited nuclear clearance (Fig. 1*B* and *SI Appendix, Fig. S1 D and E*). Upon oxidant H<sub>2</sub>O<sub>2</sub> treatment, nuclear TDP-43 was markedly reduced in abundance in colorectal epithelial cell NCM460 and became exported to the cytosol, where it colocalized with stress granule marker G3BP1 (Fig. 1*C and D* and *SI Appendix, Fig. S1F*). Simultaneously, the protein levels of both overall and nuclear TDP-43 gradually decreased with increasing H<sub>2</sub>O<sub>2</sub> concentration, while cytosolic TDP-43 became mildly up-regulated (Fig. 1*E* and *SI Appendix, Fig. S1G*). Furthermore, we found that insoluble TDP-43 decreased in a dose-dependent manner, while soluble TDP-43 increased only mildly (*SI Appendix, Fig. S1H*). In contrast, mRNA levels of *TARDBP* did not alter upon H<sub>2</sub>O<sub>2</sub> (*SI Appendix, Fig. S1I*). Consistently, TDP-43 was absent in nuclei of many epithelial cells from both UC (n = 20) or CD (n = 21) patients, accompanied by reduction in protein levels of overall and insoluble TDP-43, while mRNA levels of *TARDBP* were not altered (Fig. 1*F* and *SI Appendix, Fig. S1 J and K*). In addition, we generated acute DSS-induced colitis mouse model, which mimics UC; chronic and acute TNBS-induced experimental colitis, which mimic CD; and spontaneous colitis model in *Il10*<sup>-/-</sup> mice. Tdp-43 was absent in nuclei of intestinal epithelial cells from experimental colitis of all four mouse models and partially colocalized with stress granule marker G3BP1 (Fig. 1*G–M* and *SI Appendix, Fig. S2*). Tdp-43 nuclear clearance became more pronounced in chronic TNBS-induced colitis. Consistently, the protein levels of overall and nuclear Tdp-43 decreased over the course of colitis development (Fig. 1*G–M* and *SI Appendix,*

*Fig. S2*). These findings indicate that TDP-43 exhibits nuclear clearance and becomes reduced at the protein level in both human and mouse colitis induced by oxidative stress.

## Intestinal Epithelium-Specific Disruption of Nuclear TDP-43 Drives Severe Spontaneous Intestinal Inflammation.

Considering the importance of TDP-43 in genomic stability and RNA processing, we sought to investigate whether TDP-43 nuclear clearance is involved in IBD pathogenesis. We generated *Villin*<sup>CreERT2</sup>; *Tardbp*<sup>fl/fl</sup>(*Tardbp*<sup>iIEC-KO</sup>) mice, in which exons 2 to 3 of *Tardbp* can be inducibly deleted in intestinal epithelium upon Tamoxifen (TAM) treatment. This deletion disrupts Tdp-43 nuclear localization and RNA-processing function but does not influence its cytosolic localization (Fig. 2*A* and *SI Appendix, Fig. S3 A–C*). The gross body weight of the *Tardbp*<sup>iIEC-KO</sup> mice dropped markedly after 7 dpi. Approximately 30% of *Tardbp*<sup>iIEC-KO</sup> mice died at 8 dpi (Fig. 2*B* and *C*). Intestinal barrier dysfunction was observed in *Tardbp*<sup>iIEC-KO</sup> mice, accompanied by decreased body temperature (*SI Appendix, Fig. S3 D and E*). Four out of twelve *Tardbp*<sup>iIEC-KO</sup> mice developed obvious leaky gut at 7 dpi (*SI Appendix, Fig. S3F*). Many degenerated cells with large and round nuclei were present in *Tardbp*<sup>iIEC-KO</sup> crypts (*SI Appendix, Fig. S3G*), while the number of Paneth cells was markedly reduced (*SI Appendix, Fig. S3H*). These findings indicate that Tdp-43 is important for maintaining intestinal epithelial homeostasis.

Interestingly, all *Tardbp*<sup>iIEC-KO</sup> mice started to exhibit colitis phenotypes at 10 dpi. Their colons were characterized by disorganized epithelium, reduced colonic epithelial cells, and immune cell infiltration (Fig. 2*D*). Colitis phenotypes became more robust at 11 and 12 dpi (Fig. 2*D*). Consistently, numbers of both proliferative epithelial cells and differentiated goblet cells decreased in *Tardbp*<sup>iIEC-KO</sup> mice over time after TAM induction. Damaged epithelium had largely recovered at 13 dpi, most likely attributed to epithelial regeneration by cells that escaped *Tardbp* deletion (Fig. 2*D*). In line with these colitis phenotypes, *Tardbp*<sup>iIEC-KO</sup> mice showed higher colonoscopy scores (Fig. 2*E*), specifically in granular intestinal lumen surfaces, the presence of blood, ulcerations and abundant inflammatory fibrin exudation, and higher biochemical scores in serum (Fig. 2*F*). Inflammatory response was markedly activated in *Tardbp*<sup>iIEC-KO</sup> mice (Fig. 2*G–K* and *SI Appendix, Fig. S3I*). In addition, upon DSS treatment, *Tardbp*<sup>iIEC-KO</sup> mice developed more severe inflammation in the colon, and colitis could not be abrogated after DSS removal (*SI Appendix, Fig. S4*). Taken together, these findings demonstrate that TDP-43 mislocalization drives spontaneous colitis and enhances susceptibility to DSS-induced colitis.

## Tdp-43 Mislocalization Induces Epithelial Cell Necroptosis in the Colon.

To understand how Tdp-43 mislocalization drives colitis, we first examined cell death in the colon from *Tardbp*<sup>iIEC-KO</sup> mice at 10 dpi, when inflammation starts. Many epithelial cells in the colon were dead in *Tardbp*<sup>iIEC-KO</sup> mice (Fig. 3*A* and *B*). Interestingly, dead cells had undergone nonapoptotic cell death (Fig. 3*A* and *B*). To understand which type of cell death was induced by Tdp-43 mislocalization, we performed genome-wide transcriptome analysis of colonic epithelial cells from control (n = 3) and *Tardbp*<sup>iIEC-KO</sup> (n = 3) mice at 9 dpi, ahead of colonic inflammation. Then, 1,468 down-regulated genes and 1,457 up-regulated genes were identified in *Tardbp*<sup>iIEC-KO</sup> cells (*SI Appendix, Fig. S5A*). KEGG pathway analysis revealed that the TNF pathway was most enriched based on up-regulated gene pattern (Fig. 3*C*). Gene set enrichment analysis (GSEA) and heatmap assays further confirmed TNF signaling activation in *Tardbp*<sup>iIEC-KO</sup> mice (Fig. 3*D* and *E*). Notably, TNF signaling is critical for necroptotic cell



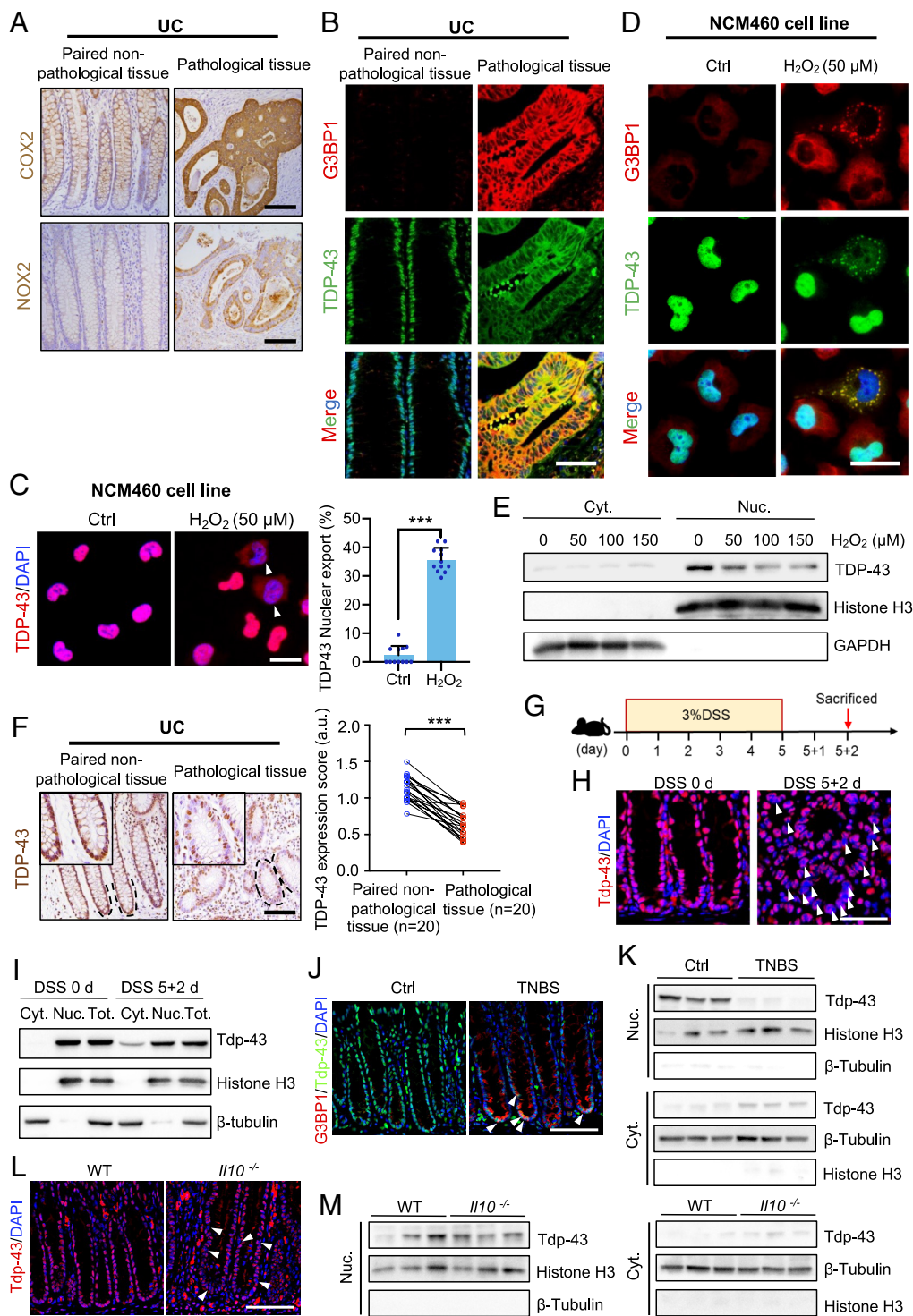


**Fig. 1.** Oxidative stress induces nuclear-to-cytosolic TDP-43 export. (A) Representative immunohistochemical images of COX2 and NOX2 in UC tissues and paired adjacent normal tissues.  $n = 20$ . (Scale bar: 100  $\mu\text{m}$ .) (B) Double immunofluorescence for TDP-43 and G3BP1 in UC tissues and paired adjacent normal tissues.  $n = 20$ . (Scale bar: 100  $\mu\text{m}$ .) (C) Immunofluorescence for TDP-43 in NCM460 cells with or without  $\text{H}_2\text{O}_2$  treatment. Arrowheads indicate TDP-43 signal in cytoplasm. The percentage of TDP-43 nuclear export was quantified.  $n = 12$ . (Scale bar: 25  $\mu\text{m}$ .) (D) Double immunofluorescence for TDP-43 and G3BP1 in NCM460 cells with or without  $\text{H}_2\text{O}_2$  treatment.  $n = 12$ . (Scale bar: 25  $\mu\text{m}$ .) (E) Western blotting for TDP-43 in nuclear and cytoplasmic proteins isolated from NCM460 cells treated with different concentrations of  $\text{H}_2\text{O}_2$ . Histone H3 and GAPDH were used as loading control for nuclear and cytoplasmic proteins, respectively. (F) Representative immunohistochemical images of TDP-43 in UC tissues and paired adjacent normal tissues. Scores reflecting TDP-43 expression levels were quantified.  $n = 20$ . (Scale bar: 100  $\mu\text{m}$ .) (G) Schematic of DSS-induced mouse acute colitis model. (H) Immunofluorescence for Tdp-43 in colon at different time points after DSS induction.  $n = 6$ . (Scale bar: 50  $\mu\text{m}$ .) (I) Western blotting for Tdp-43 in nuclear and cytoplasmic proteins isolated from colonic epithelium at different time points after DSS induction. Histone H3 and  $\beta$ -Tubulin were used as loading control for nuclear and cytoplasmic proteins, respectively. (J) Double immunofluorescence for Tdp-43 and G3BP1 in colon from chronic TNBS-induced colitis mouse model.  $n = 6$ . (Scale bar: 50  $\mu\text{m}$ .) (K) Western blotting for Tdp-43 in nuclear and cytoplasmic proteins isolated from colonic epithelium of control and chronic TNBS-induced colitis mice. Histone H3 and  $\beta$ -Tubulin were used as loading control for nuclear and cytoplasmic proteins, respectively. (L) Immunofluorescence for Tdp-43 in colon from wild-type (WT) and  $Il10^{-/-}$  mice at 20 wk of age.  $n = 6$ . (Scale bar: 50  $\mu\text{m}$ .) (M) Western blotting for Tdp-43 in nuclear and cytoplasmic proteins isolated from colonic epithelium of WT and  $Il10^{-/-}$  mice. Histone H3 and  $\beta$ -Tubulin were used as loading control for nuclear and cytoplasmic proteins, respectively. Data are presented as the mean  $\pm$  SD.  $***P < 0.001$ .

death (8). In agreement, expression of key necroptosis regulators was markedly elevated in *Tardbp*<sup>iIEC-KO</sup> mice (Fig. 3 F and G). Expression of necroptosis executioner Mlkl in 10 dpi *Tardbp*<sup>iIEC-KO</sup> colonic epithelium was strong and increased with time after TAM induction (Fig. 3H). Furthermore, *Tardbp*<sup>iIEC-KO</sup> colonic epithelial cells exhibited necrosis-like features, including fragmented nuclei and swollen mitochondria (Fig. 3I). Consistently, 4-OHT-induced Tdp-43 loss suppressed intestinal organoid growth, accompanied by a decrease in cell viability (Fig. 3J and K). *Tardbp*<sup>iIEC-KO</sup> organoids took up PI more rapidly than control organoids (Fig. 3L). Moreover, knockdown of *TARDBP* in NCM460 cells

decreased their viability and increased cytotoxicity and necrotic cells (SI Appendix, Fig. S5 B–G). Collectively, these findings demonstrate that Tdp-43 mislocalization induces necroptotic death in colonic epithelium.

**Tdp-43 Mislocalization Causes Loss of Lgr5+ Intestinal Stem Cells (ISCs).** Considering that ISCs are critical for the homeostasis and regeneration of intestinal epithelium, we sought to understand the direct effect of Tdp-43 mislocalization on ISCs. We specifically deleted *Tardbp* in *Lgr5*<sup>+</sup> ISCs using *Lgr5*<sup>GFP-creERT2</sup>; *Tardbp*<sup>fl/fl</sup> (*Tardbp*<sup>iLgr5-KO</sup>) mice. Tdp-43 mislocalization led to a remarkable reduction in *Lgr5*<sup>+</sup>

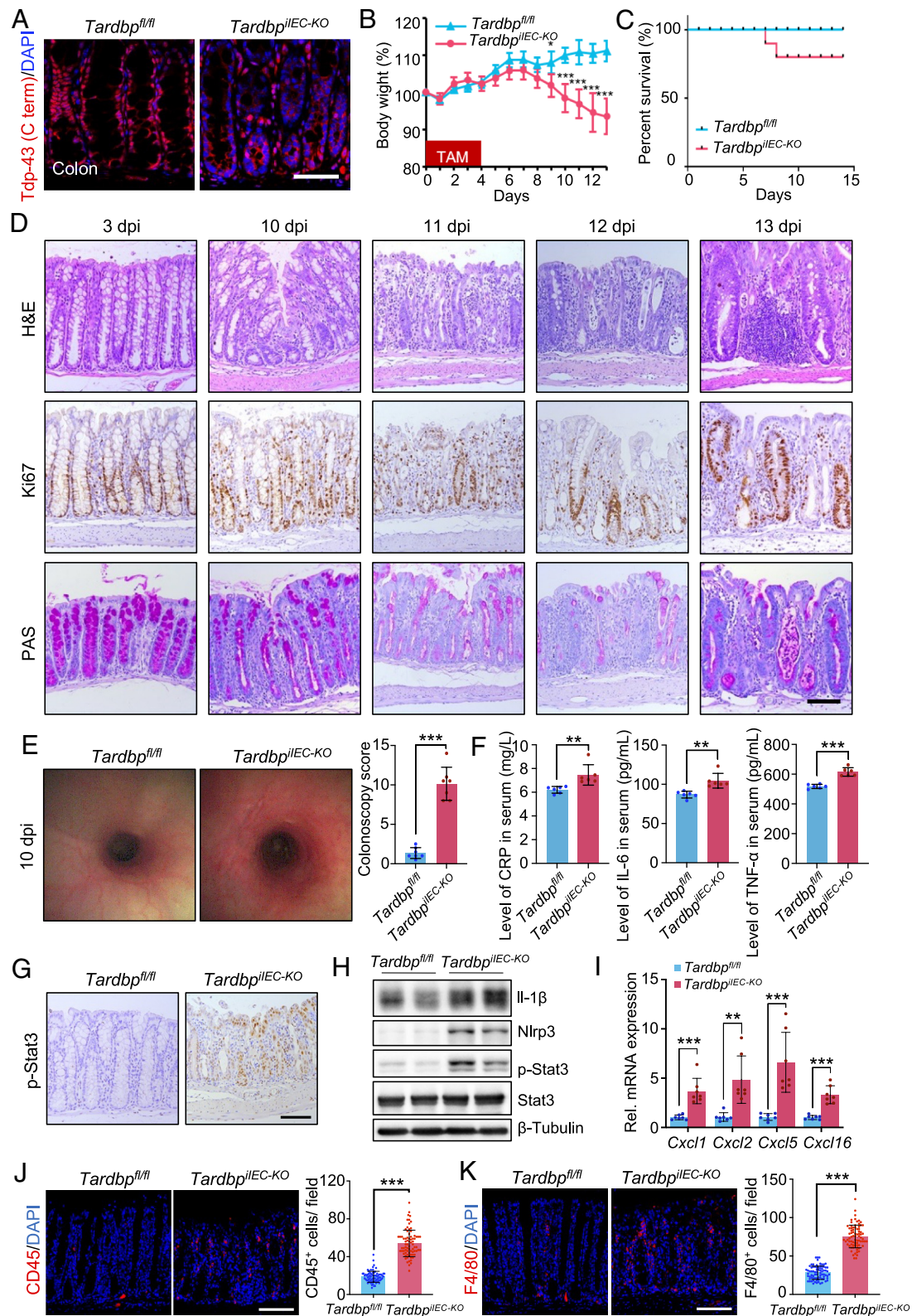


**Fig. 2.** Disruption of nuclear Tdp-43 in intestinal epithelium triggers spontaneous colitis. (A) Immunofluorescence for Tdp-43 (C-term, applied to detect Tdp-43 cytosolic localization) in colon from *Tardbp*<sup>fl/fl</sup> and *Tardbp*<sup>IEC-KO</sup> mice at 7 dpi. n = 7. (Scale bar: 50  $\mu$ m.) (B) Quantification of body weight change in *Tardbp*<sup>fl/fl</sup> and *Tardbp*<sup>IEC-KO</sup> mice after TAM injection. n = 10. (C) Kaplan–Meier survival curves of *Tardbp*<sup>fl/fl</sup> and *Tardbp*<sup>IEC-KO</sup> mice after TAM injection. n = 10. (D) Hematoxylin and eosin (H&E) staining, immunohistochemical staining for Ki67 and PAS in colon from *Tardbp*<sup>IEC-KO</sup> mice at different time points after TAM injection. n = 7. (Scale bar: 100  $\mu$ m.) (E) Representative colonoscopy images of control and *Tardbp*<sup>IEC-KO</sup> mice at 10 dpi. Colonoscopy score was quantified. n = 7. (F) ELISA analysis of CRP, IL-6 and TNF- $\alpha$  in serum from control and *Tardbp*<sup>IEC-KO</sup> mice at 10 dpi. n = 6. (G) Immunohistochemistry for p-Stat3 in colon from *Tardbp*<sup>fl/fl</sup> and *Tardbp*<sup>IEC-KO</sup> mice at 11 dpi. n = 7. (Scale bar: 100  $\mu$ m.) (H) Western blotting for Il-1 $\beta$ , Nlrp3, p-Stat3, and Stat3 in colon from *Tardbp*<sup>fl/fl</sup> and *Tardbp*<sup>IEC-KO</sup> mice at 11 dpi.  $\beta$ -Tubulin was used as loading control. (I) qRT-PCR analysis for chemokines in colon from *Tardbp*<sup>fl/fl</sup> and *Tardbp*<sup>IEC-KO</sup> mice at 11 dpi. n = 7. (J and K) Immunofluorescence for CD45 (J) and F4/80 (K) in colon from *Tardbp*<sup>fl/fl</sup> and *Tardbp*<sup>IEC-KO</sup> mice at 11 dpi. CD45<sup>+</sup> cells and F4/80<sup>+</sup> cells were quantified. n = 77 fields from seven mice. (Scale bar: 100  $\mu$ m.) Data are presented as the mean  $\pm$  SD. \*\*P < 0.01; \*\*\*P < 0.001.



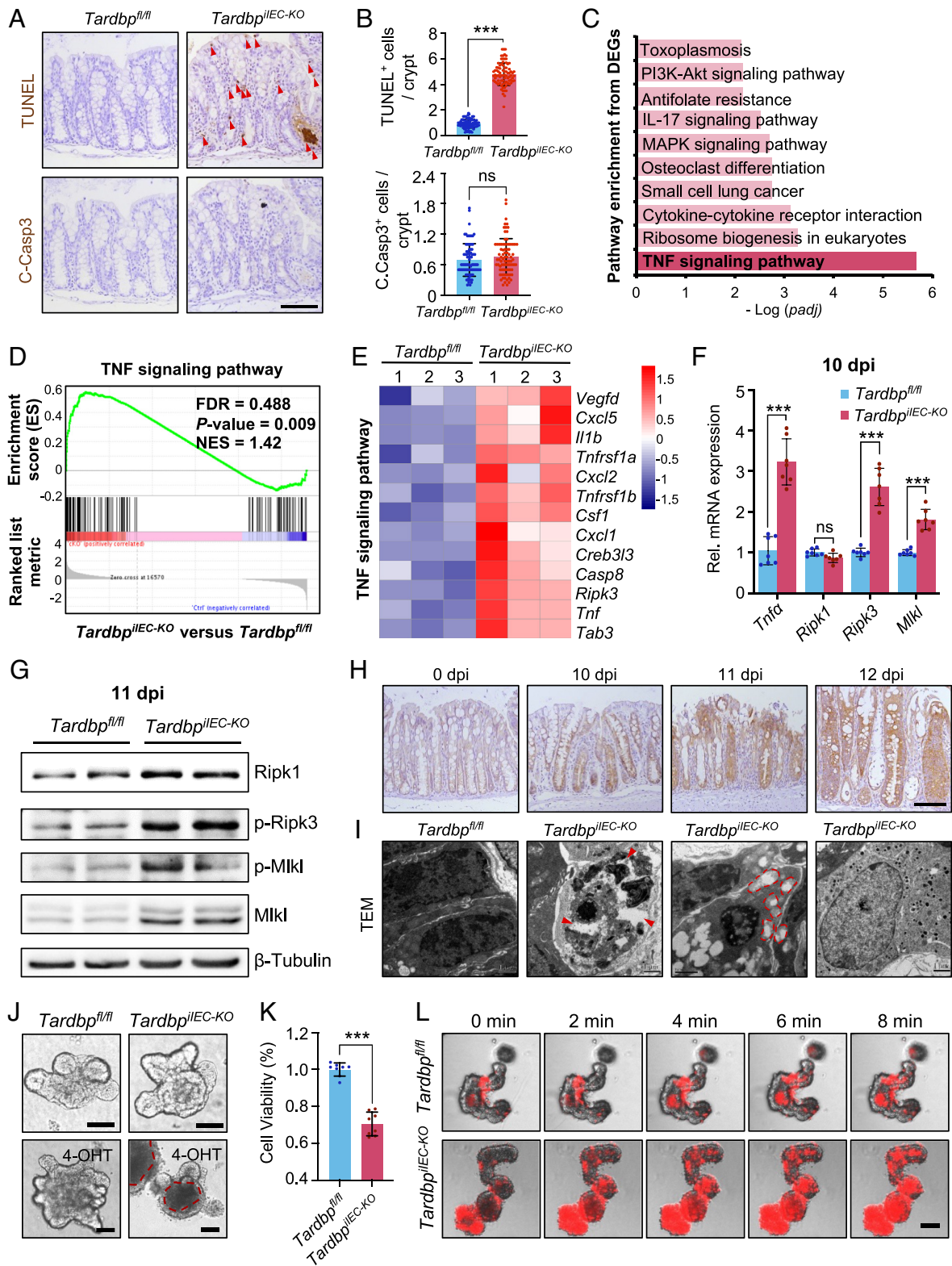


**Fig. 3.** Disruption of nuclear Tdp-43 triggers necroptosis. (A and B) Immunohistochemical staining for TUNEL and cleaved Caspase-3 in colon from *Tardbp<sup>fl/fl</sup>* and *Tardbp<sup>iEC-KO</sup>* mice at 10 dpi (A). Numbers of TUNEL<sup>+</sup> and cleaved Caspase-3<sup>+</sup> cells per crypt were quantified (B). n = 297 crypts from 6 mice. (Scale bar: 100  $\mu$ m.) (C) KEGG pathway analysis of differentially expressed genes in transcriptome profiles from *Tardbp<sup>fl/fl</sup>* and *Tardbp<sup>iEC-KO</sup>* mice at 10 dpi. n = 3. (D) GSEA of TNF-related genes in *Tardbp<sup>fl/fl</sup>* and *Tardbp<sup>iEC-KO</sup>* mice. (E) Heatmap showing altered TNF-related genes in *Tardbp<sup>fl/fl</sup>* and *Tardbp<sup>iEC-KO</sup>* mice. n = 3. (F) qRT-PCR analysis validated altered expression of necroptosis-related genes in *Tardbp<sup>fl/fl</sup>* and *Tardbp<sup>iEC-KO</sup>* mice at 10 dpi. n = 7. (G) Western blotting for necroptosis-related genes Ripk1, p-Ripk3, p-Mlkl, and Mlkl in colon from *Tardbp<sup>fl/fl</sup>* and *Tardbp<sup>iEC-KO</sup>* mice at 11 dpi.  $\beta$ -Tubulin was used as loading control. (H) Immunohistochemical staining for Mlkl in colon from *Tardbp<sup>iEC-KO</sup>* mice at indicated time points. n = 6. (Scale bar: 100  $\mu$ m.) (I) Electron microscopy images of necrotic-like colon crypt cells in 10-dpi *Tardbp<sup>iEC-KO</sup>* mice. Arrowheads indicate fragmented nuclei, dotted red lines encircle the swelling mitochondria, and a red asterisk marks low electronic condensation of cytoplasm. n = 4. TEM, transmission electron microscopy. (Scale bar: 1  $\mu$ m.) (J) Representative images of organoids from *Tardbp<sup>fl/fl</sup>* and *Tardbp<sup>iEC-KO</sup>* mice before and after 4-OHT induction. Red lines mark cells that are undergoing anoikis. n = 6. (Scale bar: 100  $\mu$ m.) (K) Cell viability analysis of organoids from *Tardbp<sup>fl/fl</sup>* and *Tardbp<sup>iEC-KO</sup>* mice 48 h after 4-OHT induction. n = 8. (L) Time-series images of organoids from *Tardbp<sup>fl/fl</sup>* and *Tardbp<sup>iEC-KO</sup>* mice 48 h after 4-OHT induction in the presence of PI (red). n = 6. Data are presented as the mean  $\pm$  SD. \*\*\*P < 0.001.

and Olfm4<sup>+</sup> cells (*SI Appendix, Fig. S6 A–F*). Lgr5<sup>+</sup> ISCs were largely absent in 4-OHT-induced organoids from *Tardbp*<sup>Lgr5<sup>+</sup> KO</sup> mice (*SI Appendix, Fig. S6G*). Furthermore, lineage tracing assay showed that Lgr5<sup>+</sup>-labeled cells gave rise to fully labeled crypt-villus ribbons in *Lgr5*<sup>GFP-creERT2</sup>; *R26*<sup>loxP-tdT</sup> *Tardbp*<sup>fl/fl</sup> mice 4 d after three pulses of TAM. In comparison, far fewer labeled crypt-villus ribbons were found in *Lgr5*<sup>GFP-creERT2</sup>; *R26*<sup>loxP-tdT</sup> *Tardbp*<sup>fl/fl</sup> mice (*SI Appendix, Fig. S6 H and I*). These findings demonstrate that Tdp-43 mislocalization causes loss of Lgr5<sup>+</sup> ISCs.

**Blocking Necroptosis Rescues Tdp-43 Mislocalization-Induced Spontaneous Colitis.** Next, we investigated whether necroptosis functionally caused spontaneous colitis observed in *Tardbp*<sup>iIEC-KO</sup> mice. Since *Mkl1* is the key necroptosis effector (23), we generated *Tardbp*<sup>iIEC-KO</sup>; *Mkl1*<sup>-/-</sup> mice, in which necroptotic activation is blocked (*SI Appendix, Fig. S7 A and B*). Body weight of *Tardbp*<sup>iIEC-KO</sup> mice dropped rapidly with time after TAM induction, while it continued to increase in *Tardbp*<sup>iIEC-KO</sup>; *Mkl1*<sup>-/-</sup> mice, matching the trend exhibited by control mice (*SI Appendix, Fig. S7C*). Over 30% of *Tardbp*<sup>iIEC-KO</sup> mice died after 7 dpi, while 100% of *Tardbp*<sup>iIEC-KO</sup>; *Mkl1*<sup>-/-</sup> mice survived (*SI Appendix, Fig. S7D*). The clinical score for colitis restored to near-normal levels in *Tardbp*<sup>iIEC-KO</sup>; *Mkl1*<sup>-/-</sup> mice (*SI Appendix, Fig. S7E*). Morphology of colonic epithelium from *Tardbp*<sup>iIEC-KO</sup>; *Mkl1*<sup>-/-</sup> mice became organized and similar to that of littermate controls (*SI Appendix, Fig. S7F*). Numbers of proliferative epithelial cells per crypt in *Tardbp*<sup>iIEC-KO</sup>; *Mkl1*<sup>-/-</sup> mice were higher than these in control mice but lower than these in *Tardbp*<sup>iIEC-KO</sup> mice (*SI Appendix, Fig. S7 G and H*). Inflammatory response was also suppressed in *Tardbp*<sup>iIEC-KO</sup>; *Mkl1*<sup>-/-</sup> mice (*SI Appendix, Fig. S7 I–L*). These findings demonstrate that blocking necroptosis rescues colitis phenotypes of *Tardbp*<sup>iIEC-KO</sup> mice.

**DNA Damage-Induced NAD<sup>+</sup> Depletion Activates Mitochondria-Dependent Necroptosis.** Zbp1 can trigger RIPK3-dependent necroptosis upon Z-form nucleic acids (24, 25). To test whether Tdp-43 mislocalization activates necroptosis in a Zbp1-dependent manner, we deleted *Zbp1* from *Tardbp*<sup>iIEC-KO</sup> mice. Deletion of *Zbp1* in intestinal epithelium could not rescue colitis phenotypes of *Tardbp*<sup>iIEC-KO</sup> mice (*SI Appendix, Fig. S8*). This suggests that Tdp-43 mislocalization-induced necroptotic activation is independent of Zbp1.

Necroptosis can be activated by DNA damage-induced PARylation overactivation in a mitochondria-dependent manner (26, 27). Considering that TDP-43 is critical for maintaining genome stability (20, 21), we thus investigated whether *Tardbp* deficiency triggers necroptosis by inducing genome instability. Gene Ontology analysis showed that intrinsic apoptotic signaling pathway in response to DNA damage was enriched among up-regulated genes in *Tardbp*<sup>iIEC-KO</sup> mice (Fig. 4A and *SI Appendix, Fig. S9A*). Upon Tdp-43 mislocalization, intestinal epithelial cells displayed euchromatin state (Fig. 4B and *SI Appendix, Fig. S9B*).  $\gamma$ -H2A.X, a marker for DNA double-strand break (DSB) foci, was significantly increased in both jejunum and colon upon *Tardbp* deficiency (Fig. 4B and *SI Appendix, Fig. S9C*), and numbers of  $\gamma$ -H2A.X<sup>+</sup> cells increased with time after TAM induction (Fig. 4C and D and *SI Appendix, Fig. S9D*). Furthermore, silencing *TARDBP* caused 3.4-fold increase in average olive tail moment in NCM460 cells, suggesting enhancement of DNA damage (Fig. 4E). Poly(ADP-ribose) (PAR) is rapidly synthesized at sites of DNA damage, including both DSBs and single-strand breaks, by the enzyme PARP1 using NAD<sup>+</sup>, which facilitates repair of damaged DNA (28). Consistently, PARP1 activity, represented by the ratio of PAR to PARP1, dramatically increased in *TARDBP*-deficient

NCM460 cells, which was accompanied by increase in  $\gamma$ -H2A.X levels (Fig. 4F–I). In contrast, transfection with 1  $\mu$ g of TDP-43-overexpressing vector, which was selected as a safe dose (*SI Appendix, Fig. S10 A–D*), resulted in nuclear localization of TDP-43 and significantly rescued *TARDBP* knockdown-induced increase in  $\gamma$ -H2A.X and PAR (*SI Appendix, Fig. S10 E–G*). This suggests that nuclear TDP-43 is important for genome stability. Furthermore,  $\gamma$ -H2A.X and PAR signals were specifically present in TDP-43<sup>+</sup> epithelial cells in human IBD tissues, while no such signals were observed in TDP-43<sup>+</sup> epithelial cells (Fig. 4J and K). These findings demonstrate that TDP-43 nuclear clearance causes DNA damage in IBD tissues.

The hyperactivation of PARP1 and excessive PAR synthesis lead to intracellular NAD<sup>+</sup> pool depletion and ATP loss, consequently promoting cell death (26). In agreement with this idea, suppression of *TARDBP* significantly reduced both NAD<sup>+</sup> and ATP levels (Fig. 5A–D). It has been reported that NAD<sup>+</sup> consumption upon DNA damage triggers metabolic shift to oxidative phosphorylation over glycolysis (29). Consistently, mitochondrial NAD<sup>+</sup> levels become elevated due to the increase of oxidative phosphorylation (Fig. 5E), suggesting compromised mitochondrial metabolism and impaired antioxidant capacity (30). The addition of exogenous NAD<sup>+</sup> significantly reduced protein levels of  $\gamma$ -H2A.X and partially rescued *TARDBP* knockdown cell viability. This was accompanied by an increase in PAR without a change in PARP1 (Fig. 5F and G). ALKBH7, an  $\alpha$ -ketoglutarate dioxygenase in mitochondria, prevents recovery of cellular NAD<sup>+</sup> levels after DNA damage-induced PARP hyperactivation, mediating necroptosis (31). To further test this mechanism, we generated *ALKBH7*-deficient 293T cells (Fig. 5H and *SI Appendix, Fig. S11 A and B*). NAD<sup>+</sup> was restored to normal baseline levels in *TARDBP* knockdown cells upon *ALKBH7* deletion (Fig. 5I). Consequently, deleting *ALKBH7* rescued reduced cell viability and increase cytotoxicity caused by *TARDBP* deficiency (Fig. 5J and K and *SI Appendix, Fig. S11C*) and restricted opening of MPT pores (Fig. 5L and M). Taken together, our data indicate that DNA damage-induced NAD<sup>+</sup> depletion mediates necroptosis caused by TDP-43 nuclear clearance.

Furthermore, both  $\gamma$ -H2A.X and p-MLKL signals were strongly present in samples from both UC and CD pathological tissues but were barely detectable in paired nonpathological tissues (*SI Appendix, Fig. S12 A–F*). TDP-43 levels were negatively associated with  $\gamma$ -H2A.X and p-MLKL in both UC and CD patients (Fig. 5N and O). NAD<sup>+</sup> levels were markedly reduced in the inflamed epithelium from both UC patients and CD patients (Fig. 5P). Considering that oxidative stress induces TDP-43 mislocalization and reduction, we concluded that *TARDBP* deficiency-induced mitochondria-dependent epithelial cell necroptosis mediates oxidative stress-driven IBD pathogenesis.

**TDP-43 Mislocalization-Induced DNA Damage Is Caused by Excessive Accumulation of R-Loops.** TDP-43 plays critical roles in RNA-processing pathways (32), and abnormally processed RNAs lead to excessive R-loops that trigger genome instability and DNA damage (33). To understand how TDP-43 mislocalization induces DNA damage, we first analyzed accumulation of genomic R-loops in NCM460 cells using anti-DNA:RNA hybrid S9.6 antibody and found that *TARDBP* inhibition markedly increased nuclear S9.6 signal intensity. To further examine whether increased S9.6 signal was due to the accumulation of R-loops, we treated NCM460 epithelial cells with RNase H endonuclease to specifically digest RNA:DNA hybrids. RNase H treatment dramatically reduced S9.6 signal intensity (Fig. 6A and B), suggesting that TDP-43 dysfunction leads to excessive accumulation of R-loops. TDP-43



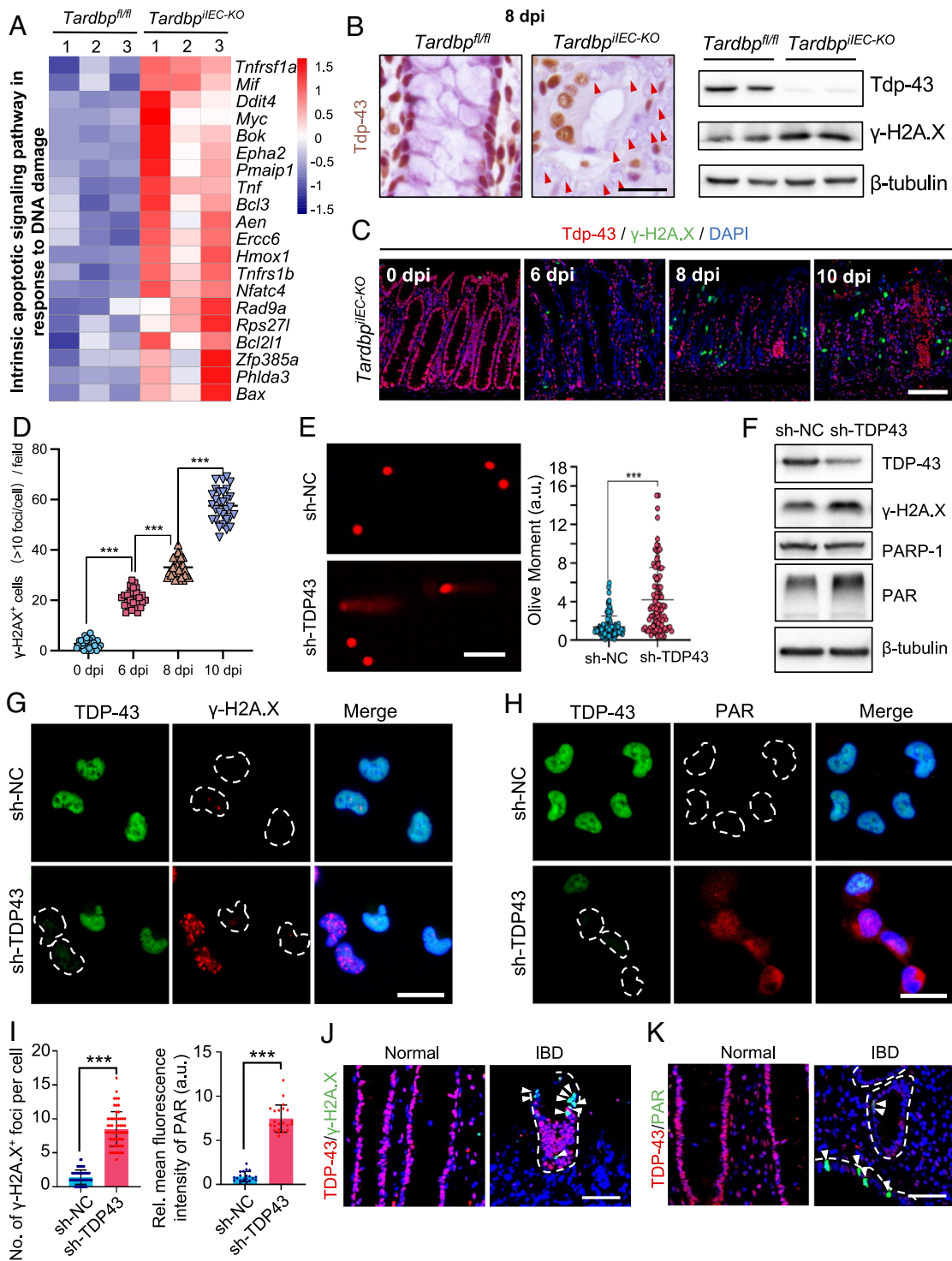


**Fig. 4.** TDP-43 disruption causes genome instability and DNA damage. (A) Heatmap showing altered genes of the intrinsic apoptotic signaling pathway in response to DNA damage in transcriptome profiles of *Tardbp*<sup>fl/fl</sup> and *Tardbp*<sup>IEC-KO</sup> mice. *n* = 3. (B) *Left panel*: immunohistochemical staining for Tdp-43 in colon from *Tardbp*<sup>fl/fl</sup> and *Tardbp*<sup>IEC-KO</sup> mice at 8 dpi. Arrowheads indicate nuclei with light hematoxylin staining of Tdp-43<sup>+</sup> cells. *n* = 7. (Scale bar: 25  $\mu$ m.) *Right panel*: Western blotting for Tdp-43 and  $\gamma$ -H2A.X in colon from *Tardbp*<sup>fl/fl</sup> and *Tardbp*<sup>IEC-KO</sup> mice at 8 dpi.  $\beta$ -Tubulin was used as loading control. (C and D) Double immunofluorescence for Tdp-43 and  $\gamma$ -H2A.X in colon from *Tardbp*<sup>IEC-KO</sup> mice at indicated time points (C). The number of  $\gamma$ -H2A.X<sup>+</sup> cells per field was quantified (D). *n* = 30 fields from six mice. (Scale bar: 100  $\mu$ m.) (E) DNA damage levels of NCM460 cells infected with sh-NC or sh-TDP43 were evaluated by the comet assay. Representative images (*Left*) and quantification of mean olive tail moment (*Right*) (*n* = 104 nuclei) are shown. (Scale bar: 50  $\mu$ m.) (F) Western blotting for TDP-43,  $\gamma$ -H2A.X, PARP-1, and PAR in NCM460 cells infected with sh-NC or sh-TDP43.  $\beta$ -Tubulin was used as loading control. (G) Double immunofluorescence for TDP-43 and  $\gamma$ -H2A.X in NCM460 cells infected with sh-NC or sh-TDP43. Dotted white lines encircled locations of the hidden nuclei. (Scale bar: 25  $\mu$ m.) (H) Double immunofluorescence for TDP-43 and PAR in NCM460 cells infected with sh-NC or sh-TDP43. Dotted white lines encircled locations of hidden nuclei. (Scale bar: 25  $\mu$ m.) (I) Number of  $\gamma$ -H2A.X<sup>+</sup> foci per cell in panel G (*n* = 65 cells for sh-NC and *n* = 83 cells for sh-TDP43) and relative mean fluorescence intensity of PAR per field in panel H (*n* = 21 fields for sh-NC and *n* = 23 fields for sh-TDP43) were quantified. (J) Double immunofluorescence for TDP-43 and  $\gamma$ -H2A.X in colon from healthy people and IBD patients. Arrowheads indicate TDP-43<sup>+</sup> and  $\gamma$ -H2A.X<sup>+</sup> intestinal epithelial cells. *n* = 20. (Scale bar: 50  $\mu$ m.) (K) Double immunofluorescence for TDP-43 and PAR in colon from healthy people and IBD patients. Arrowheads indicate TDP-43<sup>+</sup> and PAR<sup>+</sup> intestinal epithelial cells. *n* = 20. (Scale bar: 50  $\mu$ m.) Data are presented as the mean  $\pm$  SD. \*\*\**P* < 0.001.

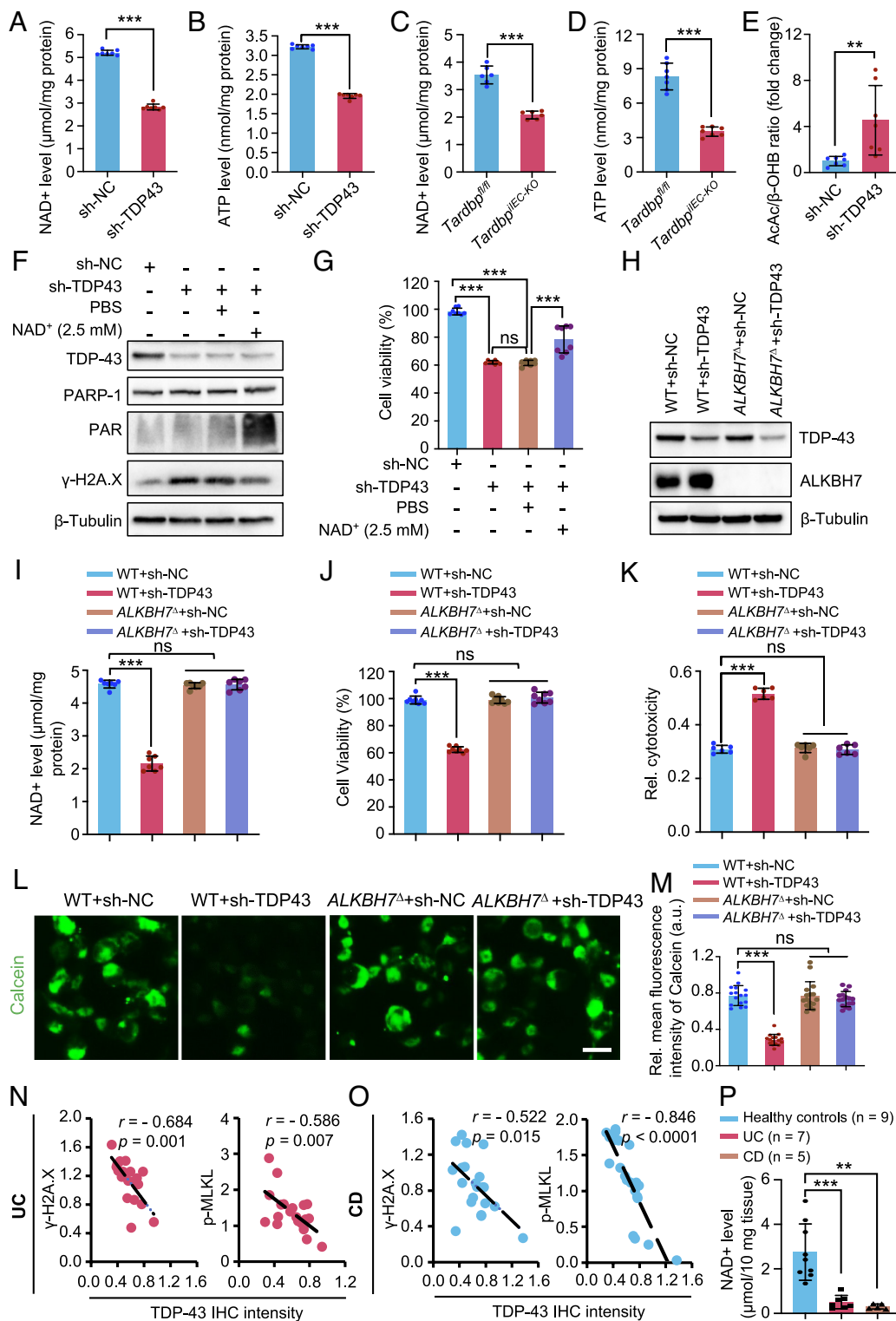


**Fig. 5.** TDP-43 nuclear clearance activates mitochondrion-dependent necroptosis. (A) NAD<sup>+</sup> level analysis of NCM460 cells infected with sh-NC or sh-TDP43. n = 7. (B) ATP level analysis of NCM460 cells infected with sh-NC or sh-TDP43. n = 7. (C) NAD<sup>+</sup> level analysis of colonic epithelial cells from *Tardbp<sup>fl/fl</sup>* and *Tardbp<sup>IEC-KO</sup>* mice at 10 dpi. n = 6. (D) ATP level analysis of colonic epithelial cells from *Tardbp<sup>fl/fl</sup>* and *Tardbp<sup>IEC-KO</sup>* mice at 10 dpi. n = 7. (E) AcAc/β-OHB ratio of NCM460 cells infected with sh-NC or sh-TDP43. n = 7. (F) Western blotting for TDP-43, HA, γ-H2A.X, PARP-1, and PAR in NCM460 cells infected with sh-NC or sh-TDP43 with and without NAD<sup>+</sup> treatment. n = 8. (G) Cell viability analysis of NCM460 cells infected with sh-NC or sh-TDP43 with and without NAD<sup>+</sup> treatment. n = 8. (H) Western blotting for TDP-43 and ALKBH7 in wild type (WT) or *ALKBH7<sup>-/-</sup>* 293T cell lines infected with sh-NC or sh-TDP43. β-Tubulin was used as loading control. (I) NAD<sup>+</sup> level analysis of WT or *ALKBH7<sup>-/-</sup>* cells infected with sh-NC or sh-TDP43. n = 7. (J and K) Cell viability analysis (J, n = 8) and LDH cytotoxicity analysis (K, n = 6) of WT or *ALKBH7<sup>-/-</sup>* cells infected with sh-NC or sh-TDP43. (L and M) Mitochondrial calcein-AM retention assay in WT or *ALKBH7<sup>-/-</sup>* cells infected with sh-NC or sh-TDP43 (L). The relative mean fluorescence intensity of calcein was quantified (M). n = 16. (Scale bar: 25 μm.) (N) Spearman correlation analysis of TDP-43 and γ-H2A.X (Left,  $P = 0.001$ ;  $r = 0.684$ ) or TDP-43 and p-MLKL (Right,  $P = 0.007$ ;  $r = 0.586$ ) in clinical UC patient samples. n = 20. (O) Spearman correlation analysis of TDP-43 and γ-H2A.X (Left,  $P = 0.015$ ;  $r = 0.522$ ) or TDP-43 and p-MLKL (Right,  $P < 0.0001$ ;  $r = 0.846$ ) in clinical CD patient samples. n = 21. (P) NAD<sup>+</sup> level analysis of healthy control tissues (n = 9) and pathological tissues from clinical UC (n = 7) and CD (n = 5) patients. Data are presented as the mean ± SD. \*\*\* $P < 0.001$ .

dysfunction-induced R-loop accumulation was further confirmed in genomic DNA isolated from NCM460 cells. Furthermore, we performed S9.6 dot blot assay with colonic epithelial cells isolated from *Tardbp<sup>IEC-KO</sup>* mice at 7 dpi, immediately before the emergence of γ-H2A.X signal. Consistent with the in vitro data, R-loop intensity was significantly enhanced in *Tardbp<sup>IEC-KO</sup>* mice (Fig. 6 C–F). Moreover, *TARDBP* inhibition significantly enhanced enrichment of R-loops (Fig. 6G). Consistently, R-loop intensity was markedly enhanced in inflamed tissues from IBD patients (Fig. 6 H

and I). Taken together, these findings provide compelling evidence that TDP-43 dysfunction causes significant excessive R-loops that can induce DNA damage in colonic epithelial cells.

**Supplementation with NAD<sup>+</sup> and NMN Alleviates *Tardbp* Deficiency-Induced Spontaneous Colitis.** Our findings indicate that excessive R-loop-induced NAD<sup>+</sup> depletion is critical for IBD onset. We thus asked whether supplementation with NAD<sup>+</sup> could alleviate *Tardbp* deficiency-induced spontaneous colonic





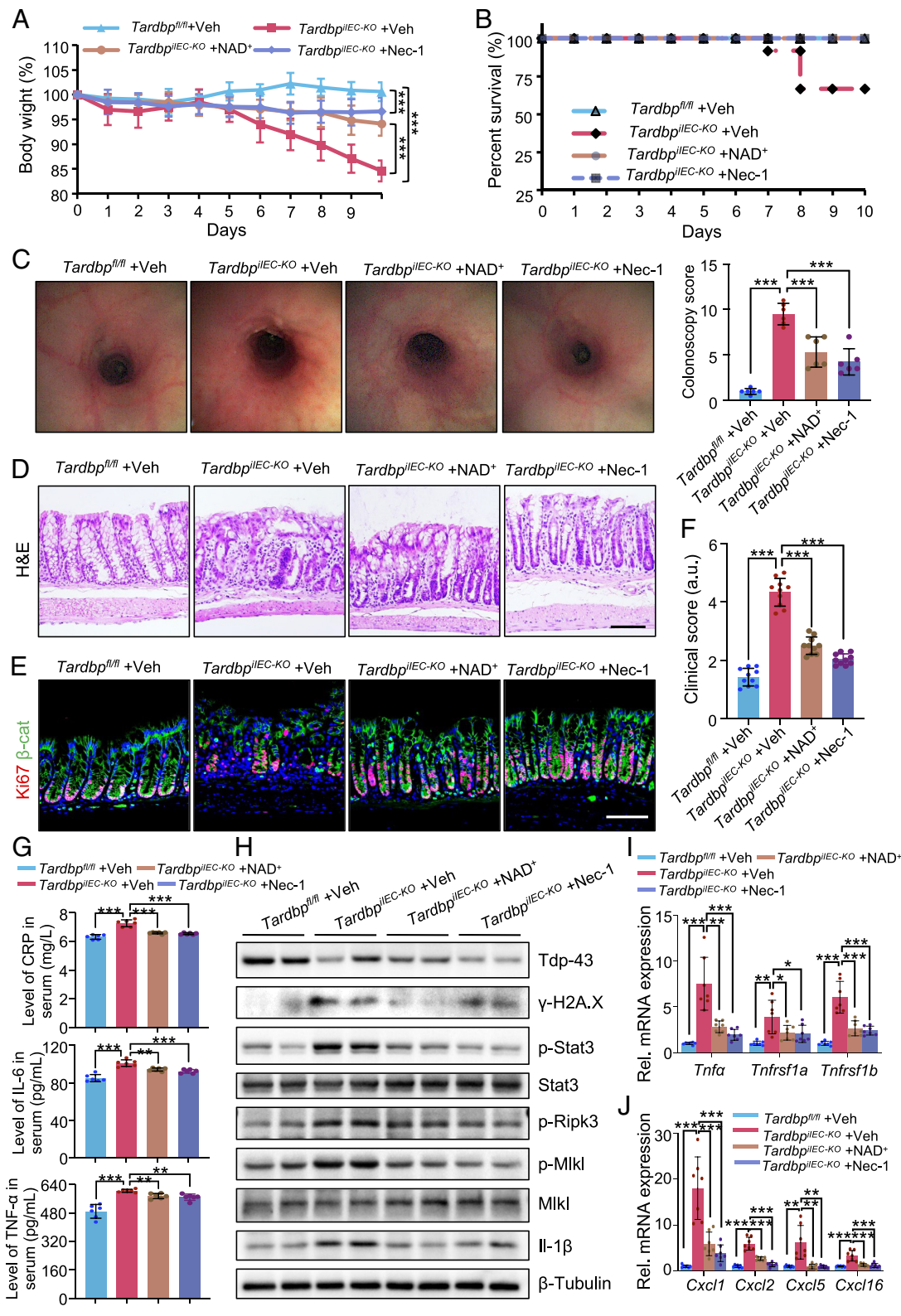


**Fig. 7.** NAD<sup>+</sup> supplementation can alleviate *Tardbp* deficiency-induced spontaneous colitis. (A) Quantification of body weight change in *Tardbp<sup>fl/fl</sup>* or *Tardbp<sup>IEC-KO</sup>* mice with NAD<sup>+</sup> or Nec-1 treatment after the first TAM injection. n = 8. (B) Kaplan-Meier survival curves of *Tardbp<sup>fl/fl</sup>* or *Tardbp<sup>IEC-KO</sup>* mice with NAD<sup>+</sup> or Nec-1 treatment after the first TAM injection. n = 8. (C) Representative colonoscopy images of *Tardbp<sup>fl/fl</sup>* and *Tardbp<sup>IEC-KO</sup>* mice with NAD<sup>+</sup> or Nec-1 treatment at 11 dpi. Colonoscopy score was quantified. n = 6. (D and E) H&E staining (D) and double immunofluorescence for Ki67 and  $\beta$ -catenin (E) in colon from *Tardbp<sup>fl/fl</sup>* or *Tardbp<sup>IEC-KO</sup>* mice with NAD<sup>+</sup> or Nec-1 treatment at 11 dpi. n = 10. (Scale bar: 100  $\mu$ m.) (F) Quantification of the clinical scores in *Tardbp<sup>fl/fl</sup>* or *Tardbp<sup>IEC-KO</sup>* mice treated with NAD<sup>+</sup> or Nec-1 at 11 dpi. n = 10. (G) ELISA analysis of CRP, IL-6 and TNF- $\alpha$  in serum from *Tardbp<sup>fl/fl</sup>* and *Tardbp<sup>IEC-KO</sup>* mice with NAD<sup>+</sup> or Nec-1 treatment at 11 dpi. n = 6. (H) Western blotting of Tdp-43,  $\gamma$ -H2A.X, Il-1 $\beta$ , p-Stat3, Stat3, and necroptosis related genes p-Ripk3, p-Mlkl, and Mlkl in colon from *Tardbp<sup>fl/fl</sup>* or *Tardbp<sup>IEC-KO</sup>* mice treated with NAD<sup>+</sup> or Nec-1 at 11 dpi.  $\beta$ -Tubulin was used as loading control. (I and J) qRT-PCR analysis of TNF-related genes *Tnfa*, *Tnfrsf1a*, *Tnfrsf1b* (I) and validation of altered chemokines *Cxcl1*, *Cxcl2*, *Cxcl5*, *Cxcl16* (J) in colon from *Tardbp<sup>fl/fl</sup>* or *Tardbp<sup>IEC-KO</sup>* mice treated with NAD<sup>+</sup> or Nec-1 at 11 dpi. n = 7. Data are presented as the mean  $\pm$  SD. \**P* < 0.05; \*\**P* < 0.01; \*\*\**P* < 0.001.

Fig. S14 A–C). Taken together, NAD<sup>+</sup> supplementation can alleviate *Tardbp* deficiency-induced spontaneous colitis.

Analogous NAD<sup>+</sup> supplementation, its precursor NMN also rescued spontaneous colitis caused by *Tardbp* deficiency (SI Appendix, Fig. S15). Moreover, supplementation with NMN alleviated DSS-induced experimental colitis (SI Appendix, Fig. S16). Considering that NMN is the most efficient and stable form of NAD<sup>+</sup> supplementation without obvious toxic effects and has beneficial effects on a diverse

array of key physiological functions (34), our findings indicate that NMN can be used for treating IBD.

## Discussion

In this study, our findings demonstrate that oxidative stress-induced TDP-43 mislocalization causes excessive R-loops that activate intestinal epithelial cell necroptosis, resulting in spontaneous intestinal



inflammation. It provides compelling pieces of evidence in support of the notion that oxidative stress is a critical driver for the onset of intestinal inflammation. Consistent with our findings, oxidative stress is a common feature of inflamed tissues from IBD patients. Mutations in antioxidant enzyme genes, including *NOQ1*, *SOD2*, *GST*, *PON*, and *NRF2*, contribute to the risk of IBD via activation of oxidative stress (2–4). A variety of IBD environmental risk factors, such as psychological stress and cigarette smoking, can activate oxidative stress in intestinal epithelial cells (35). Thus, it turns out that oxidative stress is critical for the onset of IBD. As such, natural antioxidant compounds that exhibit ROS scavenging and inhibit pro-oxidative enzymes may be useful for IBD treatment.

It is well known that multiple TDP-43 mutations occur in ALS patients (36–38). Interestingly, both gain-of-function and loss-of-function of TDP-43 mutations can cause ALS phenotypes. In TDP-43<sup>Q331K/+</sup> knock-in mice, in which the n.991C>A (p.Q331K) mutation was introduced into murine *Tardbp* gene (39), TDP-43 does not undergo nuclear-to-cytosolic mislocalization (40) and, instead, leads to a gain of TDP-43 function due to impaired TDP-43 autoregulation. In contrast, homozygous p.A382T *TARDBP* variant (A382T TDP-43) is one of the most common missense mutation in familial ALS patients (36–38). Similar to our findings, this mutation can result in TDP-43 accumulation in the cytoplasm, TDP-43 nuclear clearance, R-loop accumulation, and compromised mitochondria (19, 41), linking R-loop-induced DNA damage to ALS pathogenesis. iPSC-derived motor neurons with TDP-43 A382T mutation are vulnerable to oxidative stress (42). TDP-43 undergoes nuclear clearance, cytosolic sequestration/aggregation, and fragmentation in motor neurons of nearly 95% of sporadic ALS patients (43, 44). Thus, the changes in motor neurons caused by TDP-43 A382T mutation are similar to the features of intestinal epithelial cells from *Tardbp*<sup>-/-</sup> mice, suggesting a potential genetic connection between ALS and IBD. To validate this point, further investigation on gut phenotypes in TDP-43<sup>A382T/A382T</sup> knock-in mouse model or ALS patients bearing A382T mutation will be required in the future.

While correlation might exist between IBD and ALS, it would require further investigation. On the one hand, negative genetic correlation between ALS and IBD has been identified (45, 46). On the other hand, emerging evidence indicates that ALS associates with symptoms in the gut, characterized by elevated intestinal inflammation, gluten sensitivity, dysbiosis, and gut immotility (47). Sessile polyp and phosphorylated TDP-43 aggregates have been observed in the gut of ALS patients (48). It is worth noting that phosphorylated TDP-43 aggregates are visualized in immune cells and neuronal cells within lamina propria of intestine, while they are not present in intestinal epithelial cells. This could explain why gut symptoms are relatively mild in ALS patients. Taken together, this merits deeper investigation of whether loss-of-function TDP-43 mutations can increase susceptibility to intestinal inflammation.

Another interesting finding was the accumulation of excessive R-loops in *Tardbp*-deficient intestinal epithelial cells, which consequently caused necroptosis-mediated intestinal inflammation. It has been reported that TDP-43 nuclear clearance causes genome instability by impairing DNA DSB repair (21) and that TDP-43 nucleic acid binding and self-assembly activities are important for inhibiting R-loop accumulation, while cytosolic TDP-43 aggregation increases R-loop accumulation and DNA damage in neurons (20). Mislocalization of mutated TDP-43 (A382T) induced R-loop accumulation and R-loop-dependent increase in DNA damage, contributing to ALS pathogenesis (19). Thus, TDP-43 mislocalization-induced R-loop accumulation could be a common pathogenic contributor to IBD and ALS. Aberrant R-loop structures have been

increasingly recognized as important contributors to a number of human diseases, including autoimmune diseases, human neurological disorders, and cancer (17). Particularly, loss of *ddx41* leads to R-loop accumulation, triggering NFκB-mediated inflammation via activation of cyclic GMP-AMP synthase-stimulator of interferon genes (STING) signaling pathway (49). This means that excessive R-loops can activate inflammatory response via distinct pathways.

Here, we found that TDP-43 mislocalization drives spontaneous intestinal inflammation by activating NAD<sup>+</sup> exhaustion-induced necroptosis. Consistent with our findings, NAD<sup>+</sup> dynamics balanced by PARP1-dependent consumption and NAMPT-dependent production are important for determining the form of cell death activated under oxidative stress. When the consumption of intracellular NAD<sup>+</sup> does not recover upon oxidative stress, it induces necroptotic activation (50). Oxidative stress can also induce cell death by decreasing Nicotinamide phosphoribosyltransferase (51). In agreement, NAD<sup>+</sup> depletion alone triggers necroptosis in macrophages by directly activating RIPK3 and MLKL (52). Moreover, it has been recognized that necroptotic activation drives spontaneous ileitis and/or colitis (9, 11–13). Thus, it appears that NAD<sup>+</sup> exhaustion-induced necroptosis upon TDP-43 mislocalization-induced DNA damage is critical for the onset of intestinal inflammation. In agreement with this notion, levels of NAD<sup>+</sup> were reduced in inflamed tissues from UC patients (53). Thus, supplementation of NAD<sup>+</sup> or blocking necroptotic pathway with small molecules might represent a promising therapeutic strategy for IBD. Indeed, it has been reported that NMN treatment improved intestinal inflammation, reduced intestinal mucosal permeability, and restored gut flora dysbiosis in DSS-induced colitis (54). Therefore, supplementation with NMN could be an attractive future therapeutic strategy for IBD.

## Materials and Methods

Additional information is provided in *SI Appendix, Supplementary Materials and Methods*.

**Ethics Statement.** All mouse experimental procedures and protocols were evaluated and authorized by Beijing Laboratory Animal Management and were performed in strict accordance with the guidelines of the Institutional Animal Care and Use Committee of China Agricultural University (approval number: AW81212202-3-1).

**Patients and Clinical Specimens.** Colonoscopic biopsies for use as pathological and paired nonpathological samples were obtained from the colons of 20 UC and 21 CD patients. All patients were from Xiangya Hospital Central South University (Changsha, China). Each subject provided written informed consent. The diagnosis of UC and CD was based on clinical, radiological, endoscopic, and pathological examinations. Use of clinical samples, as well as review of all pertinent patient records, were approved by the Ethical Committee and Institutional Review Board of Xiangya Hospital Central South University in compliance with ethical standards and patient confidentiality.

**Mouse Strains.** The *Tardbp*-floxed mouse has been described previously (55). *Villin*<sup>CreERT</sup> mice (stock number: 020282), *Lgr5*<sup>eGFP-CreERT</sup> mice (stock number: 008875), and *R26*<sup>Isl1-tdT</sup> mice (stock number: 007914) were obtained from the Jackson Laboratory. *Mkl1* KO mice were obtained from Zhengxing Ying's laboratory at China Agricultural University. *Zbp1* KO mice and *Il10* KO mice were purchased from the Shanghai Model Organisms Center (stock number: NM-KO-2112761; NM-KO-190426). Mice were housed under SPF conditions with 14-h light/10-h dark cycle, and fed with a regular diet. Housing temperature is 22 °C. *Tardbp*<sup>fl/fl</sup> littermates with corn oil treatment were used as controls for *Tardbp*<sup>iEC-KO</sup> mice.

**Statistical Analysis.** At least three biologically independent experiments were performed unless stated otherwise. All data are presented as the mean ± SD. The

P value was obtained by unpaired two-tailed Student's *t* test, and asterisks denote statistical significance (\**P* < 0.05; \*\**P* < 0.01; \*\*\**P* < 0.001).

**Data, Materials, and Software Availability.** Raw fastq files for RNA-seq from this study have been submitted to the Gene Expression Omnibus (GEO; <https://www.ncbi.nlm.nih.gov/geo>) under accession number GSE227532 (56). All other data are included in the manuscript and/or *SI Appendix*.

**ACKNOWLEDGMENTS.** We thank the members of the laboratory animal center in China Agricultural University for their assistance in animal care. This study was supported by grants from the National Basic Research Program of China (2022YFA1104001, 2022YFC3602102, 2022YFD1300403, and 2021YFF1000603), the National Natural Science Foundation of China 82025006, 82230017 (to Z.Y.), 82300635 (to X.Y.), 82000498, 82270588 (to C.L.), 88220019 (to X.L.), and the Postdoctoral Science Foundation of China 2022M723412 (to X.Y.).

1. E. Martini, S. M. Krug, B. Siegmund, M. F. Neurath, C. Becker, Mend your fences: The epithelial barrier and its relationship with mucosal immunity in inflammatory bowel disease. *Cell Mol. Gastroenterol. Hepatol.* **4**, 33–46 (2017).
2. T. Arisawa *et al.*, Nrf2 gene promoter polymorphism is associated with ulcerative colitis in a Japanese population. *Hepatology* **55**, 394–397 (2008).
3. A. Karban *et al.*, Paraoxonase (PON)1 192R allele carriage is associated with reduced risk of inflammatory bowel disease. *Dig. Dis. Sci.* **52**, 2707–2715 (2007).
4. G. Guan, S. Lan, Implications of antioxidant systems in inflammatory bowel disease. *Biomed. Res. Int.* **2018**, 1290179 (2018).
5. X. Z. Shi, P. F. Lindholm, S. K. Sarma, NF- $\kappa$ B activation by oxidative stress and inflammation suppresses contractility in colonic circular smooth muscle cells. *Gastroenterology* **124**, 1369–1380 (2003).
6. C. Pereira *et al.*, DNA damage and oxidative DNA damage in inflammatory bowel disease. *J. Crohns Colitis* **10**, 1316–1323 (2016).
7. Y. Gong *et al.*, The role of necroptosis in cancer biology and therapy. *Mol. Cancer* **18**, 100 (2019).
8. S. He, X. Wang, RIP kinases as modulators of inflammation and immunity. *Nat. Immunol.* **19**, 912–922 (2018).
9. C. Gunther *et al.*, Caspase-8 regulates TNF- $\alpha$ -induced epithelial necroptosis and terminal ileitis. *Nature* **477**, 335–339 (2011).
10. M. P. Pierdomenico *et al.*, Necroptosis is active in children with inflammatory bowel disease and contributes to heighten intestinal inflammation. *Am. J. Gastroenterol.* **109**, 279–287 (2014).
11. P. S. Welz *et al.*, FADD prevents RIP3-mediated epithelial cell necrosis and chronic intestinal inflammation. *Nature* **477**, 330–334 (2011).
12. R. Wang *et al.*, Gut stem cell necroptosis by genome instability triggers bowel inflammation. *Nature* **580**, 386–390 (2020).
13. Y. Xie *et al.*, Gut epithelial TSC1/mTOR controls RIPK3-dependent necroptosis in intestinal inflammation and cancer. *J. Clin. Invest.* **130**, 2111–2128 (2020).
14. N. C. Kaneider, A. Kaser, Prostanoids put a brake on necroptosis in IBD. *Nat. Cell Biol.* **23**, 680–681 (2021).
15. Z. Y. Liu *et al.*, Necrostatin-1 reduces intestinal inflammation and colitis-associated tumorigenesis in mice. *Am. J. Cancer Res.* **5**, 3174–3185 (2015).
16. M. Zhou *et al.*, ABIN3 negatively regulates necroptosis-induced intestinal inflammation through recruiting A20 and restricting the ubiquitination of RIPK3 in inflammatory bowel disease. *J. Crohns Colitis* **15**, 99–114 (2021).
17. T. García-Muse, A. Aguilera, R. Loops: From physiological to pathological roles. *Cell* **179**, 604–618 (2019).
18. M. P. Crossley, M. Bocek, K. A. Cimprich, R-loops as cellular regulators and genomic threats. *Mol. Cell* **73**, 398–411 (2019).
19. M. Giannini *et al.*, TDP-43 mutations link amyotrophic lateral sclerosis with R-loop homeostasis and R-loop-mediated DNA damage. *PLoS Genet.* **16**, e1009260 (2020).
20. M. Wood *et al.*, TDP-43 dysfunction results in R-loop accumulation and DNA replication defects. *J. Cell Sci.* **133**, jcs244129 (2020).
21. J. Mitra *et al.*, Motor neuron disease-associated loss of nuclear TDP-43 is linked to DNA double-strand break repair defects. *Proc. Natl. Acad. Sci. U.S.A.* **116**, 4696–4705 (2019).
22. F. Gasset-Rosa *et al.*, Cytoplasmic TDP-43 de-mixing independent of stress granules drives inhibition of nuclear import, loss of nuclear TDP-43, and cell death. *Neuron* **102**, 339–357.e7 (2019).
23. A. L. Samson *et al.*, MLKL trafficking and accumulation at the plasma membrane control the kinetics and threshold for necroptosis. *Nat. Commun.* **11**, 3151 (2020).
24. H. Jiao *et al.*, Z-nucleic acid sensing triggers ZBP1-dependent necroptosis and inflammation. *Nature* **580**, 391–395 (2020).
25. T. Zhang *et al.*, Influenza Virus Z-RNAs Induce ZBP1-Mediated Necroptosis. *Cell* **180**, 1115–1129.e13 (2020).
26. L. Du *et al.*, Intra-mitochondrial poly(ADP-ribosylation) contributes to NAD<sup>+</sup> depletion and cell death induced by oxidative stress. *J. Biol. Chem.* **278**, 18426–18433 (2003).
27. W. X. Zong, D. Ditsworth, D. E. Bauer, Z. Q. Wang, C. B. Thompson, Alkylating DNA damage stimulates a regulated form of necrotic cell death. *Genes Dev.* **18**, 1272–1282 (2004).
28. M. C. Caron *et al.*, Poly(ADP-ribose) polymerase-1 antagonizes DNA resection at double-strand breaks. *Nat. Commun.* **10**, 2954 (2019).
29. M. M. Murata *et al.*, NAD<sup>+</sup> consumption by PARP1 in response to DNA damage triggers metabolic shift critical for damaged cell survival. *Mol. Biol. Cell* **30**, 2584–2597 (2019).
30. B. O'Rourke, D. Ashok, T. Liu, Mitochondrial Ca<sup>2+</sup> in heart failure: Not enough or too much? *J. Mol. Cell Cardiol.* **151**, 126–134 (2021).
31. D. Fu, J. J. Jordan, L. D. Samson, Human ALKBH7 is required for alkylation and oxidation-induced programmed necrosis. *Genes Dev.* **27**, 1089–1100 (2013).
32. E. Buratti, F. E. Baralle, TDP-43: Gumming up neurons through protein-protein and protein-RNA interactions. *Trends Biochem. Sci.* **37**, 237–247 (2012).
33. A. Aguilera, T. Garcia-Muse, R loops: From transcription byproducts to threats to genome stability. *Mol. Cell* **46**, 115–124 (2012).
34. J. Yoshino, J. A. Baur, S.-I. Imai, NAD<sup>+</sup> Intermediates: The Biology and Therapeutic Potential of NMN and NR *Cell Metabolism* **27**, 513–528 (2018).
35. D. K. Sahoo *et al.*, Oxidative stress, hormones, and effects of natural antioxidants on intestinal inflammation in inflammatory bowel disease. *Front Endocrinol. (Lausanne)* **14**, 1217165 (2023).
36. E. Kabashi *et al.*, TARDBP mutations in individuals with sporadic and familial amyotrophic lateral sclerosis. *Nat. Genet.* **40**, 572–574 (2008).
37. L. Corrado *et al.*, High frequency of TARDBP gene mutations in Italian patients with amyotrophic lateral sclerosis. *Hum. Mutat* **30**, 688–694 (2009).
38. S. Orrù *et al.*, High frequency of the TARDBP p.Ala382Thr mutation in Sardinian patients with amyotrophic lateral sclerosis. *Clin. Genet* **81**, 172–178 (2012).
39. M. A. White *et al.*, TDP-43 gains function due to perturbed autoregulation in a Tardbp knock-in mouse model of ALS-FTD. *Nat. Neurosci.* **21**, 552–563 (2018).
40. E. S. Arnold *et al.*, ALS-linked TDP-43 mutations produce aberrant RNA splicing and adult-onset motor neuron disease without aggregation or loss of nuclear TDP-43. *Proc. Natl. Acad. Sci. U.S.A.* **110**, E736–745 (2013).
41. G. Zanini *et al.*, Mitochondrial and Endoplasmic Reticulum Alterations in a Case of Amyotrophic Lateral Sclerosis Caused by TDP-43 A382T Mutation. *Int. J. Mol. Sci.* **23**, 11881 (2022).
42. A. Onda-Ohto *et al.*, Specific vulnerability of iPSC-derived motor neurons with TDP-43 gene mutation to oxidative stress. *Mol. Brain* **16**, 62 (2023).
43. I. R. Mackenzie *et al.*, Pathological TDP-43 distinguishes sporadic amyotrophic lateral sclerosis from amyotrophic lateral sclerosis with SOD1 mutations. *Ann. Neurol.* **61**, 427–434 (2007).
44. M. Neumann *et al.*, Ubiquitinated TDP-43 in frontotemporal lobar degeneration and amyotrophic lateral sclerosis. *Science* **314**, 130–133 (2006).
45. R. Zeng *et al.*, Investigating Causality and Shared Genetic Architecture between Neurodegenerative Disorders and Inflammatory Bowel Disease. *Aging Dis.* **14**, 1349–1359 (2023).
46. C. Y. Li, T. M. Yang, R. W. Ou, Q. Q. Wei, H. F. Shang, Genome-wide genetic links between amyotrophic lateral sclerosis and autoimmune diseases. *BMC Med.* **19**, 27 (2021).
47. A. M. Martin *et al.*, Distinguishing the contributions of neuronal and mucosal serotonin in the regulation of colonic motility. *Neurogastroenterol Motil* **34**, e14361 (2022).
48. S. B. Pattle *et al.*, pTDP-43 aggregates accumulate in non-central nervous system tissues prior to symptom onset in amyotrophic lateral sclerosis: A case series linking archival surgical biopsies with clinical phenotypic data. *J. Pathol. Clin. Res.* **9**, 44–55 (2023).
49. J. T. Weinreb *et al.*, Excessive R-loops trigger an inflammatory cascade leading to increased HSPC production. *Dev. Cell* **56**, 627–640.e5 (2021).
50. T. Nishida, I. Naguro, H. Ichijo, NAMPT-dependent NAD(+) salvage is crucial for the decision between apoptotic and necrotic cell death under oxidative stress *Cell Death Discov.* **8**, 195 (2022).
51. C. Zhou, W. Ying, Oxidative stress induces cell death partially by decreasing both mRNA and protein levels of nicotinamide phosphoribosyltransferase in differentiated PC12 cells. *PeerJ* **9**, e11401 (2021).
52. D. Pajuelo *et al.*, NAD(+) Depletion Triggers Macrophage Necroptosis, a Cell Death Pathway Exploited by Mycobacterium tuberculosis. *Cell Rep.* **24**, 429–440 (2018).
53. Y. H. Kang *et al.*, Metabolic analyses reveal dysregulated NAD<sup>+</sup> metabolism and altered mitochondrial state in ulcerative colitis. *PLoS One* **17**, e0273080 (2022).
54. P. Huang *et al.*, Treatment of inflammatory bowel disease: Potential effect of NMN on intestinal barrier and gut microbiota. *Curr. Res. Food Sci.* **5**, 1403–1411 (2022).
55. L. Zhao *et al.*, TDP-43 facilitates milk lipid secretion by post-transcriptional regulation of Btn1a1 and Xdh. *Nat. Commun.* **11**, 341 (2020).
56. G. Li, X. Yang, Z. Yu Excessive, R-loop-induced mitochondrial-dependent epithelial cell necroptosis drives spontaneous intestinal inflammation. GEO. <https://www.ncbi.nlm.nih.gov/geo/query/acc.cgi?acc=GSE227532>. Deposited 16 March 2023.

Author affiliations: <sup>a</sup>Tianjian Laboratory of Advanced Biomedical Sciences, Academy of Medical Sciences, Zhengzhou University, Zhengzhou, Henan 450052, China; <sup>b</sup>State Key Laboratory of Animal Biotech Breeding, College of Biological Sciences, China Agricultural University, Beijing 100193, China; <sup>c</sup>College of Agriculture and Life Sciences, Ankang University, Ankang, Shaanxi 725000, China; <sup>d</sup>China Astronaut Research and Training Center, Beijing 100094, China; <sup>e</sup>Department of Gastroenterology, Xiangya Hospital of Central South University, Changsha, Hunan 410008, China; <sup>f</sup>Hunan International Scientific and Technological Cooperation Base of AI Computer Aided Diagnosis and Treatment for Digestive Disease, Changsha, Hunan, China; <sup>g</sup>State Key Laboratory of Genetic Resources and Evolution of Kunming Institute of Zoology, Chinese Academy of Sciences, Kunming 650223, China; <sup>h</sup>Division of Gastroenterology and Hepatology, Department of Medicine, Feinberg School of Medicine, Northwestern University, IL 60611; <sup>i</sup>Department of Developmental and Cell Biology, Sue and Bill Gross Stem Cell Research Center, Center for Complex Biological Systems, University of California, Irvine, Irvine, CA 92697; and <sup>j</sup>Key Laboratory of Precision Nutrition and Food Quality, Ministry of Education, Department of Nutrition and Health, China Agricultural University, Beijing 100193, China

Author contributions: X.Y., G.L., X.L., Z.Y., and C.L. designed research; X.Y., G.L., P.L., M.Z., K.Y., J. Xiao, Y.C., J. Xu, S.T., M.D., Y.P., M.L., X.W., R.L., X.S., Y.T., L.Y., and H.K. performed research; X.Y., G.L., B.J., Y.C., M.V.P., X.L., C.L., and Z.Y. analyzed data; and X.Y., G.L., M.V.P., C.L., and Z.Y. wrote the paper.